Myosin XI-Dependent Formation of Tubular Structures from Endoplasmic Reticulum Isolated from Tobacco Cultured BY-2 Cells[1][W][OA]

Etsuo Yokota*, Haruko Ueda, Kohsuke Hashimoto, Hidefumi Orii, Tomoo Shimada, Ikuko Hara-Nishimura, and Teruo Shimmen

Department of Life Science, Graduate School of Life Science, University of Hyogo, Harima Science Park City, Hyogo 678–1297, Japan (E.Y., K.H., H.O., T. Shimmen); and Department of Botany, Graduate School of Science, Kyoto University, Sakyo-ku, Kyoto 606–8502, Japan (H.U., T. Shimada, I.H.-N.)

The reticular network of the endoplasmic reticulum (ER) consists of tubular and lamellar elements and is arranged in the cortical region of plant cells. This network constantly shows shape change and remodeling motion. Tubular ER structures were formed when GTP was added to the ER vesicles isolated from tobacco (*Nicotiana tabacum*) cultured BY-2 cells expressing ER-localized green fluorescent protein. The hydrolysis of GTP during ER tubule formation was higher than that under conditions in which ER tubule formation was not induced. Furthermore, a shearing force, such as the flow of liquid, was needed for the elongation/extension of the ER tubule. The shearing force was assumed to correspond to the force generated by the actomyosin system in vivo. To confirm this hypothesis, the S12 fraction was prepared, which contained both cytosol and microsome fractions, including two classes of myosins, XI (175-kD myosin) and VIII (BY-2 myosin VIII-1), and ER-localized green fluorescent protein vesicles. The ER tubules and their mesh-like structures were arranged in the S12 fraction efficiently by the addition of ATP, GTP, and exogenous filamentous actin. The tubule formation was significantly inhibited by the depletion of 175-kD myosin from the S12 fraction but not BY-2 myosin VIII-1. Furthermore, a recombinant carboxyl-terminal tail region of 175-kD myosin also suppressed ER tubule formation. The tips of tubules moved along filamentous actin during tubule elongation. These results indicated that the motive force generated by the actomyosin system contributes to the formation of ER tubules, suggesting that myosin XI is responsible not only for the transport of ER in cytoplasm but also for the reticular organization of cortical ER.

Endoplasmic reticulum (ER) is a spatially continuous component throughout the cytoplasm. It is composed of structurally and functionally different subdomains and populations: the cortical ER; the cytoplasmic ER, which also extends across transvacuolar strands; and the outer nuclear envelope connected to the tubular cytoplasmic ER (Staehelin, 1997; Sparkes et al., 2009b). The cytoplasmic ER is highly dynamic and exhibits rapid streaming that is considered as the driving force for cytoplasmic streaming. Recently, an actin-based molecular motor, myosin XI, was demonstrated to be involved in this streaming in tobacco (*Nicotiana tabacum*) BY-2 cells (Yokota et al., 2009), in Arabidopsis (*Arabidopsis thaliana*) cells (Ueda et al., 2010), and in characean cells (Yamamoto et al., 2006; Nunokawa et al., 2007). The cortical ER closely associates with the cell membrane, forming a polygonal network composed of tubular and lamellar elements. In contrast to the cytoplasmic ER, the cortical ER network rarely streams and takes long-distance translocation as a whole. However, they frequently change shape and remodel themselves, such as in elongation/extension and retraction of tubular elements, gradual narrowing and disappearance of polygons, or new lamellae formation from the corners of polygons (Knebel et al., 1990; Lichtscheidl and Url, 1990). Such dynamics and remodeling motions of the cortical ER network are suppressed by treatment with the actin-depolymerizing drugs cytochalasin or latrunculin (Knebel et al., 1990; Liebe and Menzel, 1995; Boevink et al., 1998; Runions et al., 2006; Sparkes et al., 2009a, 2009c), although the network is maintained in the cortical region. The depolymerization of actin filaments further induces the disintegration of tubular ER into huge lamellae or cisternae (Knebel et al., 1990; Menzel, 1994; Liebe and Menzel, 1995) or the formation of small islands of ER lamellae at the vertices of the ER tubules (Boevink et al., 1998). Cold stress (Quader et al., 1989) or the alteration of cytosolic calcium level and distribution (Quader, 1990; Liebe and Menzel, 1995) also cause tubule conversion into huge cortical ER lamellae. When such stresses are removed, tubular elements reform from the lamellae in an actin filament-dependent manner (Quader et al.,

[1] This work was supported by a Grant-in-Aid for Special Research on Priority Areas (grant no. 19039031) and Grants-in-Aid for Special Research C (grant nos. 19570046 and 21570049).

* Corresponding author; e-mail yokota@sci.u-hyogo.ac.jp.

The author responsible for distribution of materials integral to the findings presented in this article in accordance with the policy described in the Instructions for Authors (www.plantphysiol.org) is: Etsuo Yokota (yokota@sci.u-hyogo.ac.jp).

[W] The online version of this article contains Web-only data.

[OA] Open Access articles can be viewed online without a subscription.

www.plantphysiol.org/cgi/doi/10.1104/pp.111.175018

1989; Quader, 1990). Beneath the cortical network, a corresponding network of actin bundles is found, with these bundles overlaid precisely by ER tubules (Boevink et al., 1998). Electron microscopy reveals the close and tight association of actin bundles with tubular ER in the cortical network (Quader et al., 1987; Lichtscheidl et al., 1990). These observations indicate the contribution of the actin cytoskeleton to the dynamic remodeling motions in the cortical ER in plant cells and imply the involvement of myosin in these motions, especially tubular elongation/extension. However, there is an exception in an early stage of characean internodal cell expansion, in which the microtubule-based cytoskeleton was shown to be used for organization and remodeling motions in the cortical ER network (Foissner et al., 2009).

The involvement of myosin in cortical ER remodeling is supported by the fact that a general inhibitor of myosin activity, 2,3-butane-dione monoxime (BDM), suppresses not only the stream of cytoplasmic ER but also the movement of the cortical ER network (Higaki et al., 2008; Yokota et al., 2009). The globular tail domain of Arabidopsis myosin XI-K overexpressed in tobacco leaf cells also suppressed the dynamics and remodeling motion of cortical ER (Sparkes et al., 2009a). In extruded cytoplasm from mature characean internodal cells, in which actin cables and membrane organelles are included, the tubular structures, presumably ER, move along the cables and form a membranous network consisting of these tubular elements (Kachar and Reese, 1988). The velocity of elongation/extension of tubules from preexisting cortical ER tubules in onion (*Allium cepa*) bulb epidermis cells is comparable to that of cytoplasmic streaming or organelle movement (Knebel et al., 1990; Lichtscheidl and Url, 1990). It is well known that two classes of myosins, myosin VIII and XI, are expressed in higher plants (Reddy and Day, 2001; Yamamoto, 2007). Immunocytochemical study using an antibody against myosin XI (tobacco 175-kD myosin) shows the colocalization of this myosin with cortical ER in BY-2 cells (Yokota et al., 2009), while small punctate structures of the GFP-tagged tail region of an isoform of Arabidopsis myosin VIII, ATM1, expressed in tobacco cells locates along the ER tubules and their three-way junctions in the cortical network (Golomb et al., 2008).

In the yeast *Saccharomyces cerevisiae*, Myo4p, an isoform of myosin V, and its adaptor protein She3p have been suggested to play a role in the dynamic behaviors for forming and extending ER tubules (Estrada et al., 2003). Contrary to yeast and plant cells, microtubules have been shown to be primarily responsible for ER movement, the regulation of its spatial distribution, and the formation of tubular structure in vitro and in vivo in animal cells (for review, see Vedrenne and Hauri, 2006). ER tubules are believed to be pulled out from preexisting tubules by motor proteins, kinesin, and cytoplasmic dynein, migrating along microtubules or by the polymerization of microtubules whose plus ends are associated with the ER membrane. In the fungus *Ustilago maydis*, cytoplasmic dynein supports the dynamics of the cortical ER network (Wedlich-Söldner et al., 2002). However, several pieces of evidence suggest a role for the actin cytoskeleton in the motility and dynamic behavior of ER as in animal cells. Retrograde ER movement appears to be dependent on actin filaments (Terasaki and Reese, 1994; Waterman-Storer and Salmon, 1998). In Purkinje neurons, ER is transported into the dendritic spines by myosin Va (Wagner et al., 2011). The involvement of myosin V, as well as microtubule-based motors, in the movement of ER and the formation of its tubules in vitro is revealed in metaphase extract of *Xenopus* eggs (Wöllert et al., 2002).

Intriguingly, Dreier and Rapoport (2000) showed that tubular structures are spontaneously formed and arranged into polygonal networks by fusing with each other in vitro from ER microsomes prepared from *Xenopus* eggs in the absence of cytoskeletal components when GTP was added. This result suggests the importance of intrinsic ER membrane properties for tubule formation. It was also shown that integral membrane proteins, including the reticulon family proteins DP1/Yop1p (Voeltz et al., 2006) and atlastin, a dynamin family GTPase (Hu et al., 2009), were indispensable in membrane curvature in tubules. In Arabidopsis, at least 21 isoforms of reticulon family protein (AtRTNLB1 to -21; Nziengui and Schoefs, 2009; Sparkes et al., 2009b) were identified, with some of them located in tubular cortical ER elements (Nziengui et al., 2007; Tolley et al., 2008; Sparkes et al., 2010). If the alternation of membrane properties by the reticulon family proteins and other proteins is a factor in forming ER tubules, it raises the question of why the cytoskeleton, especially the actin cytoskeleton in plant cells, is required for the formation and regulation of tubular structures of ER in vivo.

In this study, we found that tubular structures elongate and extend in vitro from the ER vesicles, which were isolated from BY-2 cells, in the presence of GTP, as in the case of ER microsomes from *Xenopus* eggs (Dreier and Rapoport, 2000; Voeltz et al., 2006). However, a shearing force is necessary for this tubular elongation/extension under our experimental conditions, suggesting a role for myosin activity in vivo. By analyzing ER tubule formation and elongation in a S12 fraction containing cytosol and microsome fractions, in which both myosins and ER vesicles are included, we further suggested that the sliding activity of myosin XI interacting with ER is important for this event.

RESULTS

Formation of Tubular Structures from GFP-ER Vesicles by GTP and Shearing Force

Isolated GFP-ER vesicle (Supplemental Fig. S2) was fragmented and vesiculated during ER preparation, and these vesicles became agglomerations (Fig. 1A; Supplemental Fig. S2). When GTP was mixed with the

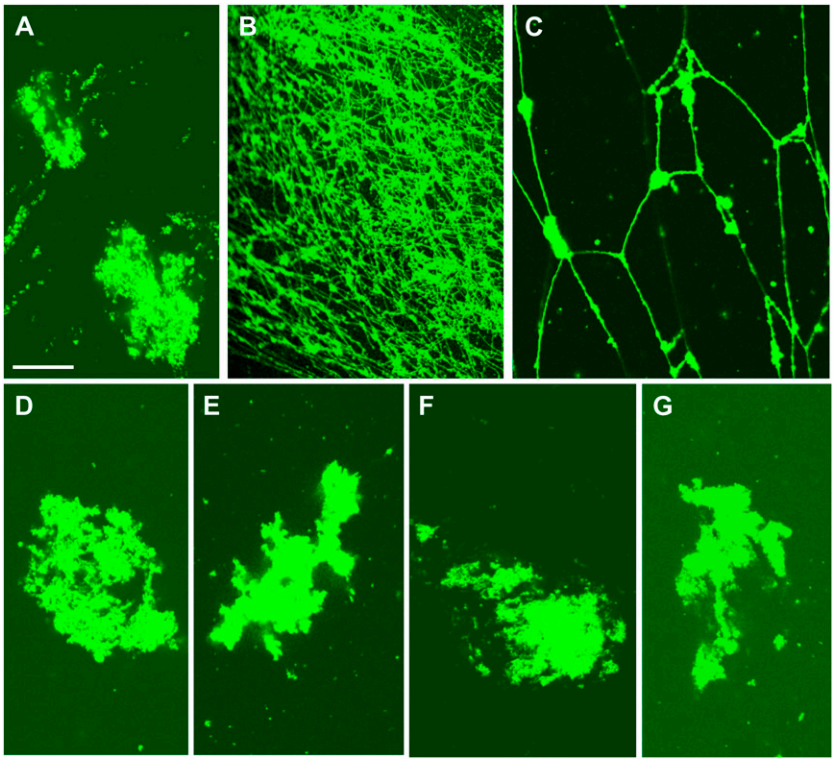

Figure 1. Formation of tubular structures from GFP-ER vesicles by GTP. GFP-ER vesicles were mixed without (A) and with 0.5 mM GTP (B and C; focused on the surface of the coverslip and in the solution, respectively), 0.5 mM GDP (D), 0.5 mM ATP (E), and 0.5 mM GTPγS (F). Tubular structures were formed from GFP-ER vesicles by GTP. When GFP-ER vesicles were pretreated with 10 μM biotin-maleimide for 10 min and then mixed with 0.5 mM GTP (G), ER tubules were not formed. Bar = 20 μm.

GFP-ER vesicles, tubular structures were formed that adhered onto the glass surface (Fig. 1B). In the flow chamber solution between the glass slide and the coverslip, mesh-like structures were frequently observed (Fig. 1C). In negative-staining electron micrographs, the tubules were not uniform throughout their length but had bulges in several places (Fig. 2, A and B). The tubule diameter ranged between 30 nm (Fig. 2A, arrow 1) and 100 nm (Fig. 2, A and B, arrow 2). Several branches were noted in the mesh-like structures, giving the appearance of several tubules emanating from same sack or vesicle (Fig. 2C). GTP at 5 μM was efficient for inducing ER tubule formation, with increased frequency and number formed at higher concentrations. By contrast, GDP (Fig. 1D), ATP (Fig. 1E), and the nonhydrolyzable GTP analog, GTPγS (Fig. 1F), could not induce tubule formation. Pretreatment of GFP-ER vesicles with a sulfhydryl reagent, biotin-maleimide, for the covalent modification of Cys residues in proteins, suppressed the tubule formation by GTP (Fig. 1G); similar suppression of tubule formation from ER microsomes by biotin-maleimide has been found in *Xenopus* eggs (Dreier and Rapoport, 2000; Voeltz et al., 2006). Conversely, an inhibitor of myosin activity, BDM, at a concentration of 50 mM, the actin-depolymerizing drug latrunculin B (LB), at a concentration of 2 μM, and the microtubule-depolymerizing drugs oryzalin and propyzamide, at concentrations of 20 and 100 μM, respectively, had no effect on the formation of ER tubules from the GFP-ER vesicles of BY-2 cells, again similar to ER microsomes of *Xenopus* eggs (Dreier and Rapoport, 2000).

During the analysis of ER tubule elongation, a shearing force, caused by the movement of the solution, was generated by mixing with GTP, applying on the glass slide, and mounting the coverslip. We noticed that the shearing force was required for the tubule elongation. Figure 3, A and B, show images of GFP-ER vesicles that had been exposed to GTP at 25°C for 1 min and 40 min, respectively. ER tubule formation was not evident, even after 40 min (Fig. 3B). However, the tubule elongation was dramatically induced in GFP-ER vesicle aggregates adhering to the glass surface when a shearing force was generated by the flow of solution within the flow chamber caused by solution adsorption by a filter paper placed at the chamber edge. Figure 3, C and D, show images before and after the generation of flow, respectively. The tubule elongation velocity corresponded to solution flow rate and ranged from several micrometers per second to tens of micrometers per second (Fig. 3E; Supplemental Fig. S3, A–D). In some cases, the elongated ER tubule shrank or retracted (Fig. 3F; Supplemental Fig. S3E) when it was not fixed to the glass surface and the flow ceased.

Hydrolysis of GTP during the ER Tubule Elongation

Since ER tubule formation was not induced by GDP addition (Fig. 1D) or GTPγS (Fig. 1F), it was hypothesized that GTP hydrolysis occurs during tubule formation. To examine this possibility, we measured GTPase activity under conditions suitable, or unsuitable, for tubule formation. For the former state, the GFP-ER vesicles were continuously stirred by a mag-

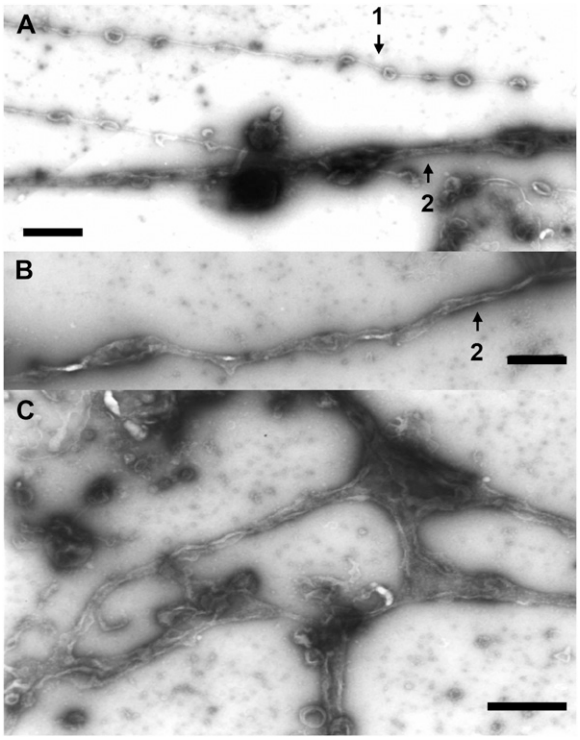

Figure 2. Negative-staining electron micrographs of GTP-treated GFP-ER vesicles. A and B, Tubular structures of approximately 30 nm (arrow 1) or 100 nm (arrows 2) diameter. C, Branching structures of several ER tubules. Bars = 500 nm.

netic stirrer after the addition of GTP (Fig. 4, A and B, black circles). For latter state, the GFP-ER vesicles were kept standing after adding GTP, then mixed gently (Fig. 4, A and B, white circles). A large number of fine ER tubules were formed under the stirred conditions (Fig. 4D), while only a few tubules were formed under unsuitable conditions (Fig. 4C). The rate of GTP hydrolysis was constant during the assay period under unsuitable conditions (Fig. 4A, white circles), estimated to be 0.068 ± 0.007 μM inorganic phosphate (Pi) μg^{-1} protein min^{-1} at 25°C from five separate measurements. On the other hand, the rate of GTP hydrolysis under suitable conditions exhibited two phases. During the early assay period, the GTP hydrolytic rate was estimated to be 0.158 ± 0.021 μM Pi μg^{-1} protein min^{-1} (Fig. 4A, black circles before 40 s), approximately double the rate under unsuitable conditions, after which the rate was similar to the unsuitable conditions (Fig. 4A, black circles after 60 s). Under the conditions favorable for ER tubule formation, pretreatment with biotin-maleimide suppressed the increase in GTP hydrolysis, with rates comparable to those found under unfavorable conditions (Fig. 4B). These results suggest that the first phase of GTP hydrolysis couples to ER tubule elongation, since during this phase tubule formation was immediately induced by the shearing force (Fig. 3). When the ER tubules were fully formed, the GTPase activity slowed to the same level as that observed under conditions where ER tubule formation did not occur.

F-Actin-Dependent ER Tubule Formation in the S12 Fraction

As described above, both GTP (Fig. 1) and shearing force were required to induce ER tubule elongation from GFP-ER vesicles under our experimental conditions (Fig. 3). In plant cells, tubule elongation in the cortical ER network has been reported to be inhibited by treatment with actin-depolymerizing drugs or myosin inhibitors, as described in the introduction. From this evidence, it was suggested that the actomyosin system contributes to the generation of the shearing force required for ER tubule elongation in vivo. To further examine the roles of actin and myosin in tubule formation, we utilized the S12 fraction (Supplemental Fig. S2), including both cytosol and microsome fractions, which contained GFP-ER vesicles that did not aggregate (Supplemental Fig. S2), even after 50 min at

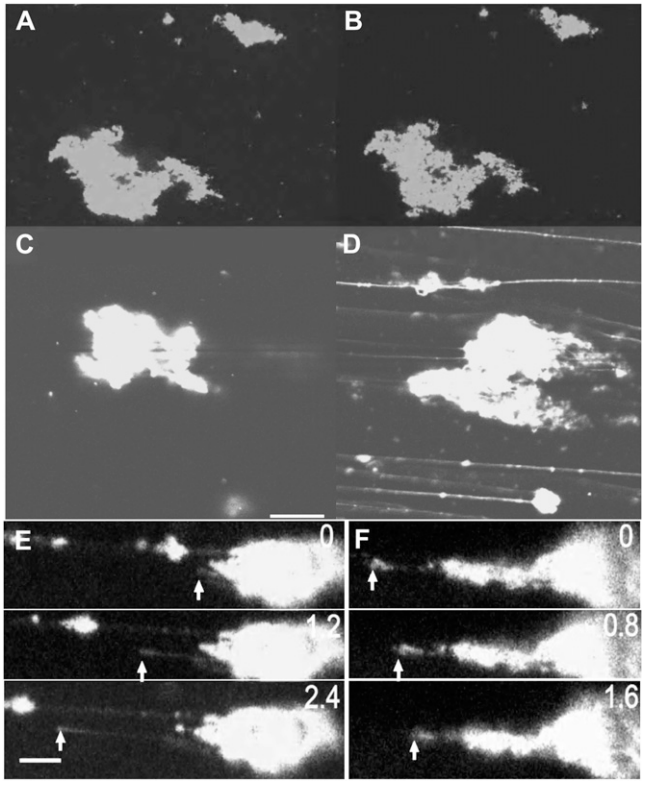

Figure 3. Elongation of ER tubules caused by shearing force. A to D, GFP-ER vesicles introduced into a flow chamber on ice with 0.5 mM GTP were kept standing at 25°C for 1 min (A) or 40 min (B and C). When a shearing force, caused by the flow of solution, was generated, the tubules elongated (D) from the GFP-ER vesicles (C). Bar = 20 μm. E and F, Time course of elongation (E) and shrinkage (F) of ER tubules. Numbers at top right are times in seconds from the commencement of recording by a CCD camera. In E, a tubule elongated (arrows) at 10 to 14 $\mu m\ s^{-1}$. In F, an elongated tubule shrank (arrows) at 7.8 $\mu m\ s^{-1}$. Bar = 10 μm.

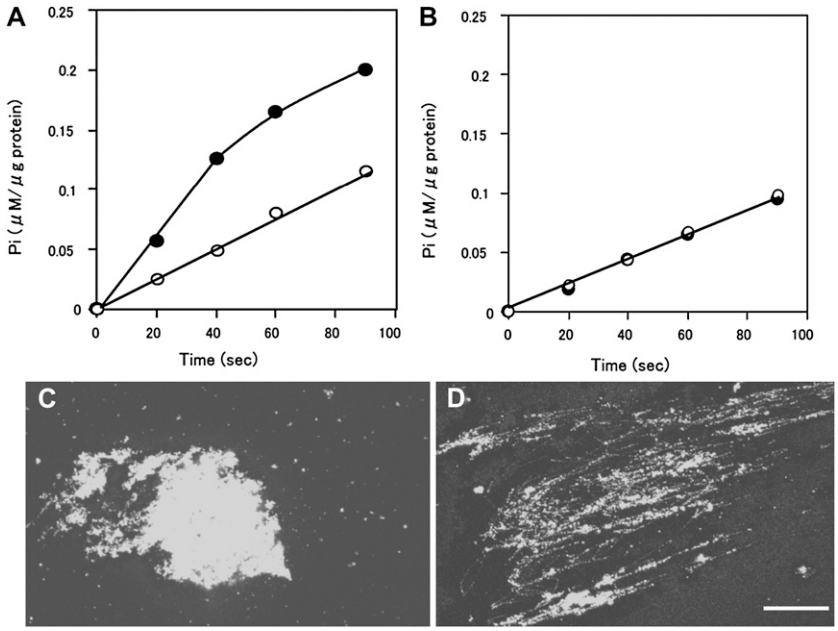

Figure 4. GTP hydrolysis during ER tubule formation. A, GTP hydrolysis by GFP-ER vesicles mixed continuously by stirring (black circles) or not (white circles) after the addition of 0.4 mM GTP. B, Effect of pretreatment of biotin-maleimide on GTP hydrolysis. GFP-ER vesicles pretreated with 10 μM biotin-maleimide for 10 min were stirred continuously (black circles) or not (white circles) after the addition of GTP. C and D, ER tubules were formed under stirring conditions (D) but not without stirring (C). Bar = 20 μm.

25°C (Fig. 5Aa). Only a few actin filaments and very short actin bundles were found when this fraction was stained with rhodamine-phalloidin (RP; Supplemental Fig. S4Ba). ER tubules and their mesh-like structures were formed and arranged when F-actin, ATP, and GTP were added to the S12 fraction (Fig. 5, Ab and B, column b). On the other hand, few tubules were found in the presence of ATP and GTP without F-actin (Fig. 5, Ac and B, column c) or GTP and F-actin without ATP (Fig. 5, Ad and B, column d). However, low levels of tubule formation were noted in the presence of F-actin and ATP without GTP (Fig. 5, Ae and B, column e). The degree of tubule formation positively correlated with the amount of added F-actin (Fig. 6). To exclude the possibility that the polymerization of endogenous actin generates the pushing force for the ER tubule elongation, we estimated actin contents in the S12 fraction and examined the effect of the reduction of actin from the S12 fraction on ER tubule formation. In the S12 fraction, endogenous actin was estimated to be 228.4 ± 28.6 nM from five separate experiments (one example is shown in Supplemental Fig. S5B). As the S12 fraction was diluted 2-fold, the final concentration of actin in the assay chamber was approximately 114.2 nM, close to the critical concentration of barbed-end F-actin, around 100 nM (Ren et al., 1997). The actin concentration in the S12 fraction after treatment with bovine serum albumin (BSA) beads was estimated at 223.4 ± 22.6 nM from five separate experiments and was similar to that in untreated S12 fraction. Even when the amount of the actin was reduced to approximately 17 nM in the S12 fraction (Supplemental Fig.

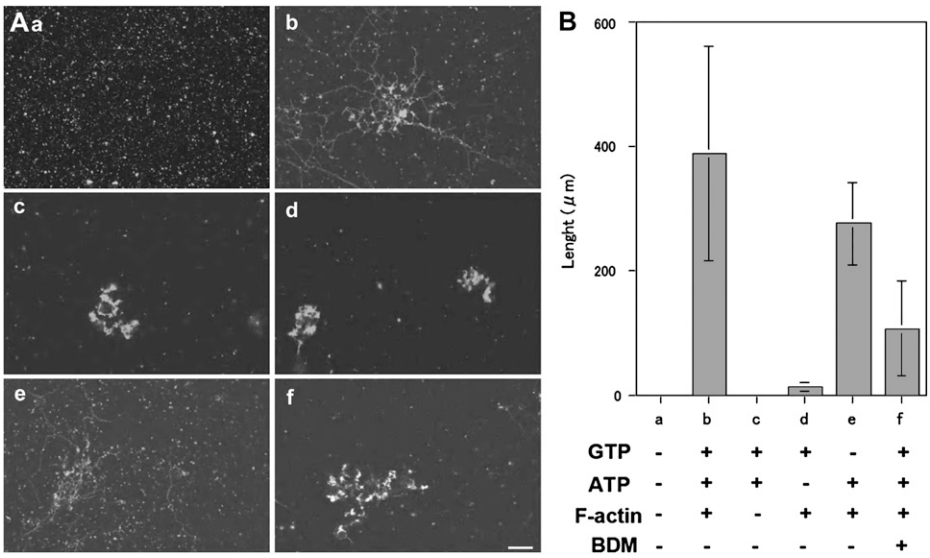

Figure 5. ER tubule formation in the S12 fraction (A) and the length of ER tubules (B). A, Images taken 50 min after each treatment: a, only S12 fraction; b, S12 fraction with 2 mM ATP, 0.5 mM GTP, and 2.5 μg mL^{-1} F-actin; c, S12 fraction with ATP and GTP but not F-actin; d, S12 fraction with GTP and F-actin but not ATP; e, S12 fraction with ATP and F-actin but not GTP; f, S12 fraction in the presence of 50 mM BDM with ATP, GTP, and F-actin. Bar = 10 μm. B, Length of ER tubules after 50 min under the same conditions as described in A. Means ± SD from three separate experiments are plotted.

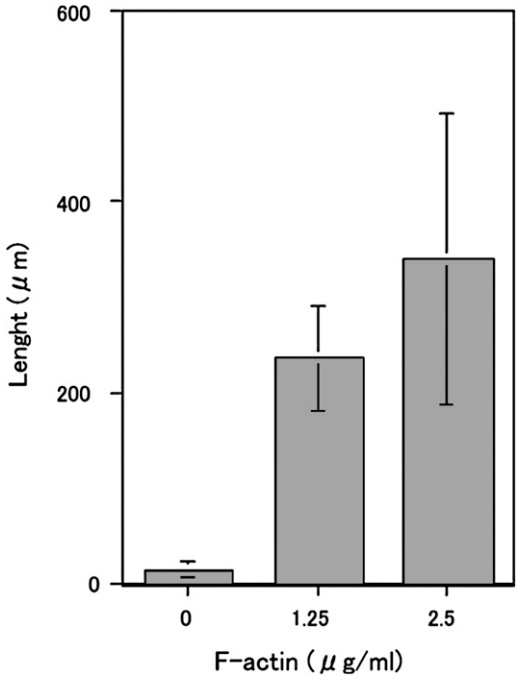

Figure 6. The length of ER tubules formed in the S12 fraction as a function of F-actin concentrations at 0, 1.25, and 2.5 μg mL^{-1} in the presence of 2 mM ATP and 0.5 mM GTP. Means ± SD from three separate experiments are plotted.

S5B; 16.2 ± 1.5 nM from five separate experiments; in the assay solution, half of the actin, 8.1 nM, was present) by DNase I beads, ER tubes were formed at similar levels to the control, which used BSA beads (Supplemental Fig. S5, C and D). Tubule formation was suppressed by the addition of BDM (Fig. 5, Af and B, column f): only 25% of control levels without BDM was found. Few ER tubules were formed when taxol-stabilized microtubules were added in the place of F-actin with ATP and GTP (Supplemental Fig. S6B). These results suggest that the ER tubule elongation induction is dependent on exogenously added F-actin, and further that myosin activity mainly contributes to ER tubule formation in the S12 fraction, in agreement with the evidence showing that maize (*Zea mays*) pollen G-actin was merely copolymerized by rabbit skeletal muscle F-actin (Jing et al., 2003).

The Presence of Two Classes of Myosins in the S12 Fraction

Two classes of myosins, myosin VIII and myosin XI, are expressed in higher plants (Reddy and Day, 2001; Yamamoto, 2007). In this study, we focused on the 175-kD myosin XI, which has been demonstrated to be involved in ER transport in BY-2 cells (Yokota et al., 2009). Myosin XI was included in the S12 fraction (Supplemental Fig. S7B, lane c). Phylogenic analysis based on the motor domain primary sequence revealed a very close relationship between the 175-kD myosin (accession no. AB082121) and *Nicotiana benthamiana* myosin XI-2 (Nb myosin XI-2; accession no. DQ87135), while the 170-kD BY-2 myosin XI (Yokota et al., 2009; accession no. AB180675) is closely related to *N. benthamiana* myosin XI-K (Nb myosin XI-K; accession no. DQ875137; Avisar et al., 2008). The primary sequence in the tail region of 175-kD myosin was also almost identical to Nb myosin XI-2 (Supplemental Fig. S1), implicating 175-kD myosin as a homolog of Nb myosin XI-2.

A 130-kD component recognized by an antibody against a recombinant ATM1 H chain protein (anti-ATM1 antibody) was present in a crude extract of Arabidopsis seedlings (Supplemental Fig. S7A, lane b) and also in the S12 fraction of BY-2 cells (Supplemental Fig. S7B, lane b). This molecular mass was consistent with the properties of ATM1 recognized in cress (*Lepidium sativum*) and maize using antibodies (Reichelt et al., 1999). To confirm whether this component is a BY-2 homolog of the myosin VIII H chain, it was isolated from immunoprecipitates with the anti-ATM1 antibody in the S12 fraction (Supplemental Fig. S7C, lane a, arrow) and assayed by mass spectrometry (MS). Polypeptide sequences from the 130-kD component (Supplemental Fig. S8A) matched those of *N. benthamiana* myosin VIII-1 (Nb myosin VIII-1; accession no. DQ875138; Avisar et al., 2008). Hence, we refer to this 130-kD component as BY-2 myosin VIII-1 hereafter.

Motile Activity in Fractions Containing BY-2 Myosin VIII

The motile and ATPase activities of myosin VIII have not yet been shown or characterized. As a first step in examining which myosin class contributes to ER tubule elongation, we examined whether BY-2 myosin VIII-1 possess the motile activity. This myosin in a crude extract from BY-2 cells bound to F-actin (Supplemental Fig. S9B, lane a) and was not dissociated from it either by washing with a low-ionic-strength solution (−KCl) containing ATP (Supplemental Fig. S9B, lane c) or by a high-ionic-strength solution (+0.3 M KCl) without ATP (Supplemental Fig. S9B, lane e). However, washing with a high-ionic-strength solution containing ATP released the myosin from F-actin (Supplemental Fig. S9B, lane f). In contrast, the 175-kD myosin bound to F-actin (Supplemental Fig. S9A, lane a) could be released from it by treatment with ATP in low-ionic-strength solution (Supplemental Fig. S9A, lane b), as shown previously (Yokota et al., 1999). The eluate of ATP containing the high-ionic-strength solution (Supplemental Fig. S9B, lane f) was subject to chromatography on a hydroxylapatite column. The BY-2 myosin VIII-1 was eluted in potassium phosphate buffers above 250 mM (Supplemental Fig. S10A, top panel), while the 175-kD myosin could be eluted using 120 to 220 mM potassium phosphate buffer (Supplemental Fig. S10A, bottom panel). The fractions containing the BY-2 myosin VIII-1 (Supplemental Fig. S10A, fractions 20–26) were subject to further chromatography on a DEAE-Sephacel column. The myosin

was eluted in solutions above 350 mM KCl (Supplemental Fig. S10B). Motile activity was found in these fractions (Supplemental Fig. S12A), in which the 175-kD myosin was not detected (Supplemental Fig. S11A, lane c). F-actin labeled with RP (RP-F-actin) moved at 0.5 to 2.4 μm s^{-1} with an average velocity of 1.2 μm s^{-1} in a conventional motility assay in vitro, in which myosin was fixed on the glass surface. This velocity was lower than reported values for myosin XI: tobacco 175-kD myosin at an average velocity of 9 μm s^{-1} (Yokota et al., 1999) or 4 μm s^{-1} (Tominaga et al., 2003); lily (*Lilium longiflorum*) pollen 170-kD myosin at an average velocity of 7.7 μm s^{-1} (Yokota and Shimmen, 1994); or the estimated sliding velocity from recombinant MYA1 motor domain of Arabidopsis at about 3 μm s^{-1} (Hachikubo et al., 2007). When the amount of BY-2 myosin VIII-1 in these fractions was reduced by immunodepletion using the anti-ATM1 antibody (Supplemental Fig. S11B, lane c), the motile activity was diminished (Supplemental Fig. S12B). Based on these results, it was likely that BY-2 myosin VIII-1 possesses the motile activity. However, the possibility that another myosin undetected by the antibodies is included in the fractions and exerts the motile activity cooperative with myosin VIII-1 is not completely excluded.

Inhibitory Effect of Immunodepletion of 175-kD Myosin from the S12 Fraction on Tubule Formation

Each myosin was depleted from the S12 fraction by immunoprecipitation using antibodies against each myosin, the anti-BM175 tail or anti-ATM1 antibody. When BY-2 myosin VIII-1 was depleted from the S12 fraction (Fig. 7Aa), ER tubules and their mesh-like structure were formed (Fig. 7, B and E, column a) in similar amounts to the controls (Fig. 7, D and E, column a). However, ER tubule formation was significantly suppressed (Fig. 7, C and E, column b) when the amount of 175-kD myosin in the S12 fraction was reduced (Fig. 7Ab). Only about 12% of control levels of ER tubules were found in the immunodepleted S12 fraction, in which 9.8% to 12.5% of 175-kD myosin was estimated to remain.

When the immunoprecipitated 175-kD component (Supplemental Fig. S7D, lane a, arrow) with the anti-BM175 tail antibody was analyzed by MS, peptide sequences from this component closely matched the 175-kD myosin and Nb myosin XI-2 H chain (Supplemental Fig. S8B), while other tobacco myosins belonging to class XI were not detected. To further confirm the involvement of 175-kD myosin in ER tubule formation in the S12 fraction, we raised an antibody (anti-BM175 peptide antibody) against a 19-amino acid peptide from the 175-kD myosin H chain (amino acids 937–955; Supplemental Fig. S1, red double arrow). This peptide sequence showed high similarity to Nb myosin XI-2, the *N. benthamiana* homolog of 175-kD myosin as described above, but low similarity to other tobacco myosin XI (Supplemental Fig. S1). In the S12 fraction, the anti-BM175 peptide antibody cross-reacted with the 175-kD polypeptide (Supplemental Fig. S7B, lane d), which exhibited a high degree of homology with the 175-kD myosin H chain in the MS analysis (Supplemental Fig. S8C). ER tubule and network formation were dramatically suppressed in the S12 fraction

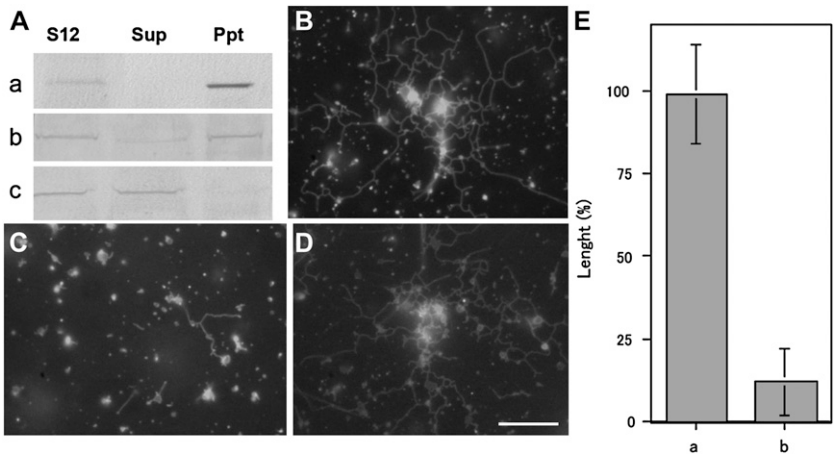

Figure 7. Effects of myosin immunodepletion from the S12 fraction on ER tubule formation. A, Immunodepletion of BY-2 myosin VIII-1 (a) or 175-kD myosin (b) from the S12 fraction by myosin H chain-specific antibodies. The S12 fraction (S12) was mixed with each antibody and then with protein A beads. After centrifugation, the supernatant (Sup) and pellet (Ppt) were recovered and then subjected to immunoblotting with the anti-ATM1 antibody (a) or 175-kD myosin H chain-specific antibodies (b). As a control, the S12 fraction was mixed only with protein A beads and then immunoblotting was carried out using a 175-kD myosin H chain-specific antibody (c). B to D, ER tubule formation in the supernatant shown in Aa, Ab, and Ac, respectively, in the presence of 2 mM ATP, 0.5 mM GTP, and 2.5 μg mL^{-1} F-actin. Bar = 10 μm. E, Columns a and b show the length of ER tubules formed in the supernatant shown in Aa and Ab, respectively. The length is shown as a relative value (%) to that of the control, and means ± SD from three separate experiments are plotted.

(Supplemental Fig. S13C), in which the 175-kD myosin was immunoprecipitated (Supplemental Fig. S13Ac, sup). These results further support the hypothesis that 175-kD myosin is required for the formation of ER tubules in the S12 fraction.

Inhibitory Effect of the C-Terminal Tail Region of 175-kD Myosin on the Tubule Formation in the S12 Fraction

To examine whether 175-kD myosin-interacting ER moves along actin filaments and generates the force for the formation and elongation of tubules, we analyzed the effect of recombinant C-terminal tail regions of this myosin including 100 amino acids (Supplemental Fig. S1, blue double arrow) fused to dihydrofolate reductase (Tominaga et al., 2003; Supplemental Fig. S14A, lane a) on the formation of ER tubules in the S12 fraction. This recombinant tail protein contained a C-terminal portion of dilute domain (Supplemental Fig. S1, red underline) and a putative AtRab-binding sequence, FLLD, which was also conserved in other tobacco myosin XI isoforms (Supplemental Fig. S1, red bracket; Hashimoto et al., 2008), and was anticipated to exert a dominant negative effect on the interaction of endogenous 175-kD myosin with ER. Some portions of 175-kD myosin, about 35% to 43%, were associated with microsomes and recovered in the pellet after ultracentrifugation in either the absence (Supplemental Fig. S14, Ba and Ca, lanes Ppt) or the presence of control recombinant protein (Supplemental Fig. S14Cb, lane Ppt). However, the amount of this myosin recovered in the pellet was reduced to below 9% by the addition of recombinant tail protein to the S12 fraction (Supplemental Fig. S14Bb, lane Ppt), indicating that this protein has a dominant negative effect on the interaction of 175-kD myosin with microsomes and perhaps ER vesicles. Concomitantly, ER tubule formation was suppressed by the recombinant tail protein (Fig. 8, B and D, column b), whereas control recombinant protein had few inhibitory effects (Fig. 8, A and D, column a). About 40% of BY-2 myosin VIII-1 containing in the S12 fraction was recovered in the microsome fraction after ultracentrifugation, with the amount unaffected by the presence of the recombinant tail protein (Supplemental Fig. S14D).

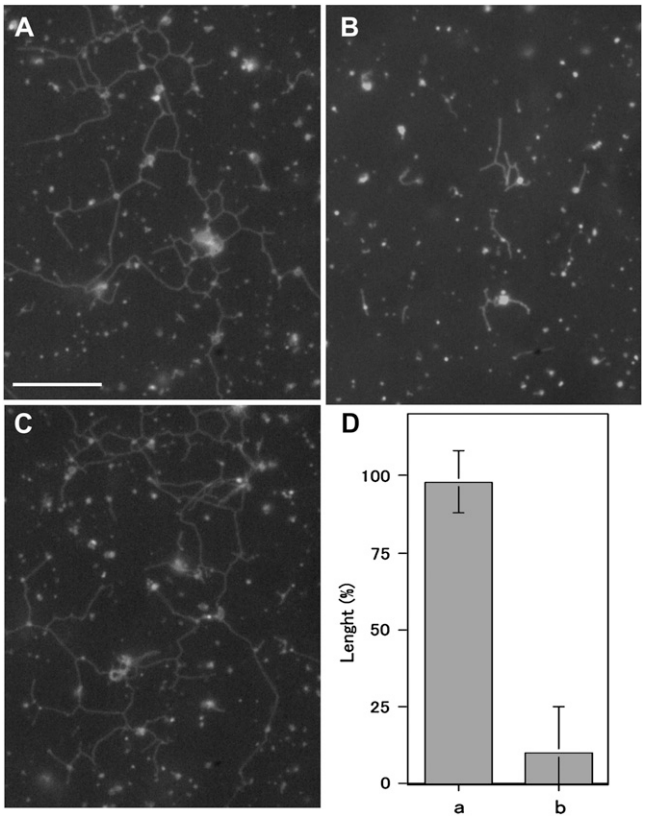

Figure 8. Effects of 175-kD myosin recombinant tail proteins on ER tubule formation in the S12 fraction. A, Control recombinant protein at a concentration of 25 μg mL^{-1}. B, Recombinant tail protein at a concentration of 20 μg mL^{-1}. C, No proteins. The control recombinant protein or the recombinant tail protein at final concentration of 25 or 20 μg mL^{-1}, respectively, was mixed with the S12 fraction, and then 2 mM ATP, 0.5 mM GTP, and 2.5 μg mL^{-1} F-actin were supplemented to the mixture. Bar = 10 μm. D, Columns a and b show the length of ER tubules formed in the presence of control recombinant protein and recombinant tail proteins, respectively. The length is shown as a relative value (%) to that in the absence of recombinant proteins, and means and ± SD from three separate experiments are plotted.

Positional Relation of ER Tubules with F-Actin in the S12 Fraction

We analyzed the positional relation of ER tubule structures with F-actin. For this purpose, RP-F-actin was added to the S12 fraction. The F-actin was arranged into bundles (Fig. 9A; Supplemental Fig. S4Bc) due to the presence of the endogenous actin-binding protein, villin (Supplemental Fig. S4A; Yokota et al., 2003). In some cases, the tubular ER coaligned with actin bundles (Fig. 9C, arrows), but not in all cases (Fig. 9C, arrowheads). Next, we tried to observe the elongation and movement of ER tubules in the S12 fraction. Higher concentrations of RP-F-actin (5 μg mL^{-1}) than those in the experiments described above were added to the S12 fraction in order to increase the opportunity to observe these events. Hence, thick and bright actin bundles were arranged that could occasionally be detected by a high-sensitivity CCD camera even in the GFP channel (Fig. 11C, arrow). Figures 10 and 11 show the time courses of elongating ER tubules. In Figure 10, the ER tubule elongated at first along an actin bundle, indicated by arrow 1 (Fig. 10, C and O), with a velocity at about 1.2 μm s^{-1} from Figure 10, A to C, and then detached from the bundle and appeared to shrink (Fig. 10D). Its tip again bound to another actin bundle (Fig. 10F), indicated by arrow 2 (Fig. 10, M and O), and it elongated along the bundle with a velocity between 1.1 and 2.8 μm s^{-1} from Figure 10, J to M. During this process, the ER tubule was bent at the intersection (Fig. 10G,

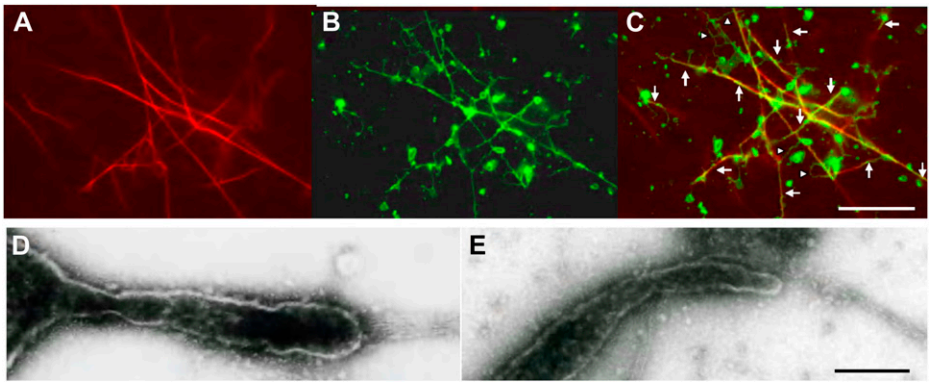

Figure 9. Positional relation of ER tubules with actin bundles in the S12 fraction. A and B, Fluorescence microscopy images of RP-F-actin (A) and tubular structures (B) 50 min after the S12 fraction was treated with 2 mM ATP, 0.5 mM GTP, and 2.5 μg mL^{-1} RP-F-actin. C, Merged image of A and B. Arrows indicate the overlapping ER tubules with actin bundles, while arrowheads do not. Bar = 10 μm. D and E, Negative-staining electron microscopy images focused on tips of ER tubules in contact with actin bundles. Bar = 200 nm.

asterisk) of actin bundles 1 and 2, and the elongating tubule overlapped with actin bundles (Fig. 10P). In Figure 11, the tubule began to elongate from an aggregate of GFP-ER vesicles apparently attached to the actin bundles, indicated by arrow 1 (Fig. 11I), or directly onto the glass surface. The tip of the tubule contacted with and slid along an actin bundle, indicated by arrow 1 (Fig. 11, H and I), with a velocity between 2.2 and 3.6 μm s^{-1}, while the main body of the tubule was apart from the bundle. In this case, the elongating tubule did not coalign with the actin bundle (Fig. 11J).

A polygonal network composed of ER tubules was frequently observed in the S12 fraction as shown above. As an ER tubule moved along an actin bundle, it would switch to move along another intersecting actin bundle, causing the ER tubule to bend (Fig. 10). If the ER tubule is not associated with actin bundles, only the tip moves along the bundle, with the main body of the tubule separate from the bundles, as shown in Figure 11. Factors responsible for the association of the ER tubule with actin bundles are suggested to be present in the S12 fraction. To close the polygon, intertubule fusion is required, although

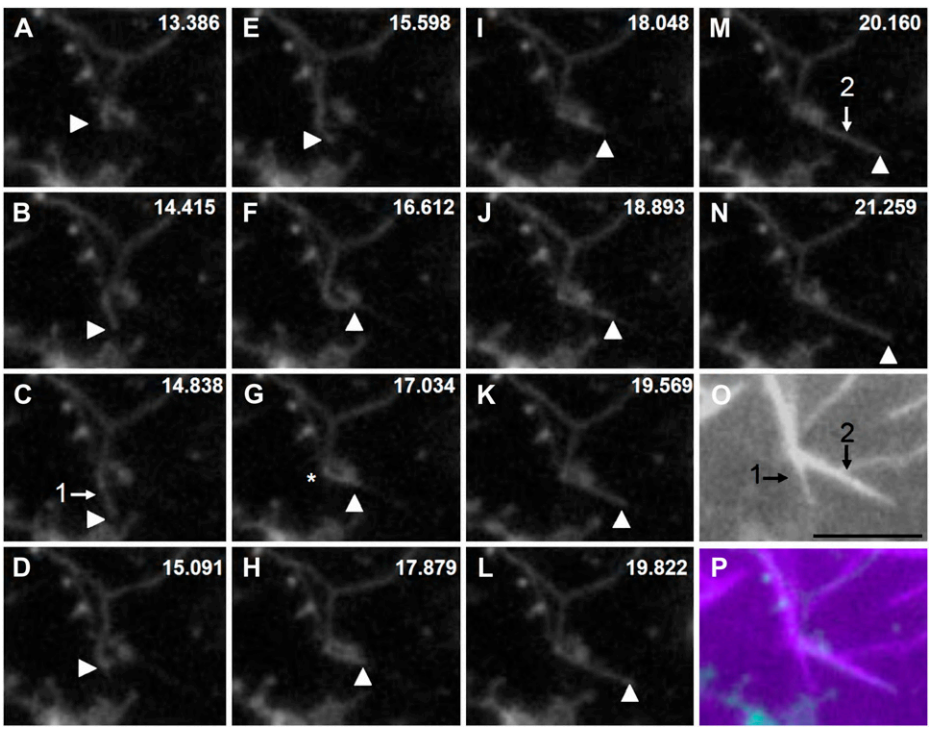

Figure 10. Sequential images of ER tubule elongation along actin bundles and the colocalization of elongated tubules along them. The S12 fraction was mixed with 2 mM ATP, 0.5 mM GTP, and 5 μg mL^{-1} RP-F-actin. The numbers at top right in A to N indicate the time in seconds. O shows an image of RP-F-actin, and P shows the merged image of N and O. The green and magenta signals show the GFP-ER and RP-F-actin, respectively. Arrowheads indicate the tip of the ER tubule. Arrows 1 in C and 2 in M indicate the positions of actin bundles shown in O. From A to C, the ER tubule slid at 1.2 μm s^{-1} along actin bundle 1, while it slid at 1.1 μm s^{-1} from J to K, 2.8 μm s^{-1} from K to L, and 1.9 μm s^{-1} from L to M along actin bundle 2. Bar = 5 μm.

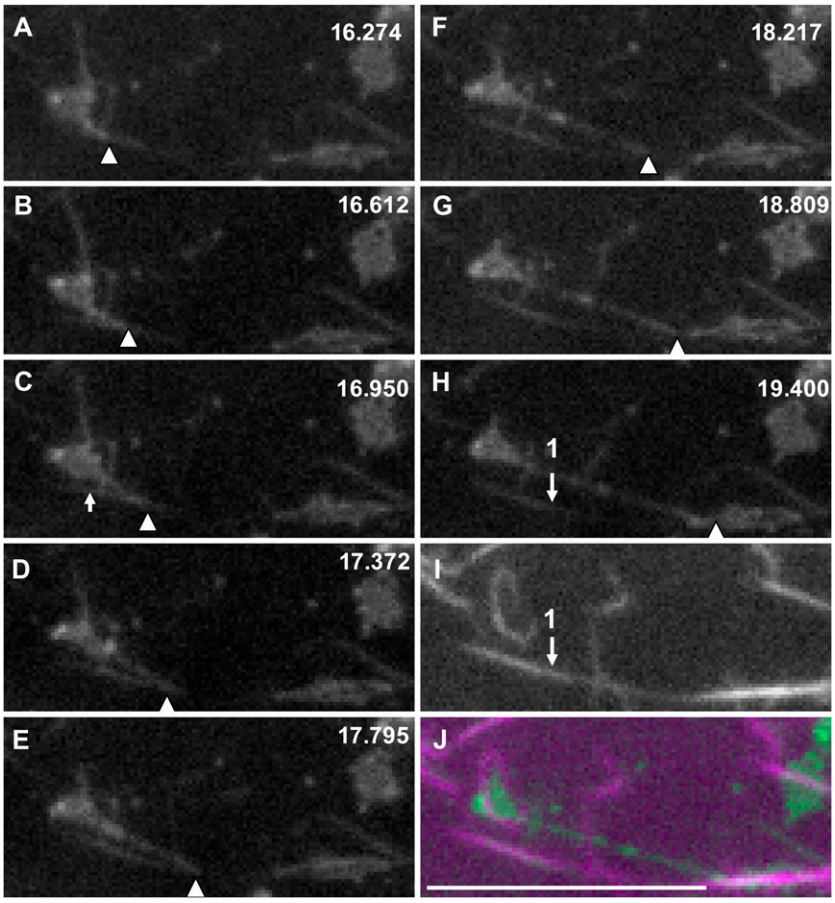

Figure 11. Sequential images of ER tubule elongation along actin bundles. The S12 fraction was mixed with 2 mM ATP, 0.5 mM GTP, and 5 μg mL^{-1} RP-F-actin. A tip-elongating ER tubule was positioned on an actin bundle. The numbers at top right in A to H indicate the time in seconds. I shows RP-F-actin, and J shows the merged image of H and I. The green and magenta signals show GFP-ER and RP-F-actin, respectively. Arrowheads indicate the tip of an elongating ER tubule. Arrow 1 in H indicates the position of the actin bundle shown in I. The arrow in C indicates a portion of the actin bundle detected in the GFP channel. The tip of the ER tubule slid along actin bundle 1 at 2.2 μm s^{-1} from C to E, 3.6 μm s^{-1} from E to F, and 2.9 μm s^{-1} from F to G. Bar = 10 μm.

this could not be observed in this study. The identification of association and fusion factors is needed to further understand the mechanism of polygonal network formation of ER tubules.

Electron Microscopic Observation of Tubular Tips Contacting with Actin Bundles

Organelles and vesicles associated with or adhering to a cortical ER tubule or its network junctions have been reported to frequently pull the ER membrane by their moving, resulting in the formation of the ER tubule in an animal cell, CV-1 cell (Lee and Chen, 1988), and a plant cell, onion inner epidermal cell (Lichtscheidl and Url, 1990). It was shown that the movement of Golgi, which appears to be associated tightly with the cortical ER network, drags the ER membrane and occasionally induces the formation of tubular ER (Brandizzi et al., 2002). A similar phenomenon occurred when pulling the Golgi on the cortical ER using optical tweezers in Arabidopsis leaf cells, in which the movement and translocation of Golgi are inhibited by LB (Sparkes et al., 2009c). These results indicate the intimate relationship between Golgi movement and the elongation of ER tubules in the cortical network and raise the possibility that the Golgi remains attached to GFP-ER vesicles and is implicated in the elongation of ER tubules in the S12 fraction. We observed tubular structures in the S12 fraction, with their tips contacting actin bundles, by electron microscopy. Figure 9, D and E, show negative-staining electron micrographs of tubule tips in contact with the actin bundles. The tips without distinct membrane structures continued to the body of the tubules, and neither additional vesicles nor patches were found at the tips. This observation provides evidence that ER tubule elongation and dynamics in the cortical network also occur in the absence of Golgi within tobacco leaves treated with brefeldin A (Sparkes et al., 2009a).

DISCUSSION

Development of an in Vitro System of Plant ER Remodeling with ER Vesicles, GTP, Myosin, and F-Actin

We developed the reconstitution system of ER tubule formation in vitro using ER vesicles isolated from BY-2 cells and showed the requirement of not only GTP but also a shearing force caused by solution flow for this event (Figs. 1 and 3). The requirement of GTP had been reported by Dreier and Rapoport (2000) and Voeltz et al. (2006) in reconstitution analyses of tubular

and reticular formation in vitro using ER microsomes isolated from *Xenopus* eggs. However, the shearing force was not necessary for the *Xenopus* system. Our system further showed that spontaneous formation and arrangement of ER tubules and their polygonal network, apparently similar to those in vivo, were induced by the addition of ATP and F-actin to the S12 fraction containing ER vesicles and myosin and were suppressed by BDM (Fig. 5). Therefore, it is suggested that ER tubule formation is an intrinsic ER membrane property that can be activated by GTP and hydrodynamic force, which is generated by the actomyosin system in the S12 fraction and in vivo.

ER tubules elongated from aggregated ER vesicles along the direction of flow with a velocity comparable to that of the solution flow rate, with a greater length than that observed in the ER network in the S12 fraction or in vivo. In the electron microscopic observations, the tubules had bulges in several places (Fig. 2). The tubule also elongated from small ER vesicles (Supplemental Fig. S3). Hence, it was conceivable that the tubules elongate ER vesicles by fusing with other ER vesicles from which tubules further elongated. In our in vitro system using isolated ER vesicles, a shearing force was continually applied to the ER vesicles adhered on a glass surface. On the other hand, the direction of elongating ER tubules and their length in the S12 fraction were dependent on the array and length of actin bundles (Figs. 10 and 11). These situations seem likely to be applicable to the ER tubule and its network formation in vivo.

GTP Hydrolysis during ER Tubule Formation

The addition of GTP is essential for efficient ER tubule formation in vitro from GFP-ER vesicles from BY-2 cells (Fig. 1). Taken together with the observations that GDP and GTPγS could not induce ER tubule formation, GTP hydrolysis is considered to be essential for ER tubule formation. In fact, the GTPase activity was detected in ER vesicles, and its activity level was correlated to ER tubule formation (Fig. 4). At present, the GTP-hydrolyzing factor(s) responsible for the in vitro formation of ER tubules from GFP-ER vesicles of BY-2 cells is uncertain. Recently, Hu et al. (2009) revealed that an atlastin protein, a family of dynamin GTPases, contributes to the formation of ER tubules in concert with reticulon proteins and DP1/Yop1p in animal and yeast cells. This protein is composed of GTP-binding and hydrolysis domains and sites at its N terminus and transmembrane domains in its C terminus. The Arabidopsis homolog, RHD3 (for root hair defective 3), was identified, with its mutant strain showing defective growth of root hairs and other root cells (Galway et al., 1997; Wang et al., 1997) and the alteration of ER morphology (Zheng et al., 2004). Instead of a fine cortical ER network, the cable-like organization often oriented parallel to the long axis of root hair cells was found in the *rhd3* mutant. It is possible that tobacco RHD3 orthologs play some roles in ER tubule formation in our system. Another possible candidate required for ER tubule formation is Rab protein of small GTPase. The Rab protein has been reported to be required for ER assembly (Turner et al., 1997; Audhya et al., 2007). Interestingly, an Arabidopsis Rab protein, AtRab8, was found to interact with Arabidopsis reticulon family proteins, AtRTNLB1, -2, and -4 (Hwang and Gelvin, 2004).

The Movement of Myosin XI Responsible for ER Tubule Formation

The S12 fraction contained the 175-kD myosin and the 130-kD component (Supplemental Fig. S7) identified as a homolog of *N. benthamiana* myosin VIII-1 (BY-2 myosin VIII-1; Supplemental Fig. S8). Decreasing the amount of 175-kD myosin by immunodepletion using antibodies raised against the myosin H chain dramatically reduced the formation of ER tubules in the S12 fraction, whereas the depletion of the BY-2 myosin VIII-1 did not (Fig. 7). Myosin XI is believed to be associated with its targeting organelles and vesicles through its C-terminal tail region, with the expressed tail region of myosin XI in living cells exerting dominantly strong negative effects on the movement and transport of organelles such as Golgi, mitochondria, and peroxisomes (Yokota and Shimmen, 2011). Consistent with this observation, the recombinant protein containing the C-terminal tail region of 175-kD myosin dissociated this myosin from microsomes (Supplemental Fig. S14) and concomitantly suppressed the formation of ER tubules and their networks in the S12 fraction (Fig. 8). The elongating ER tubules moved along the actin bundles with maximum velocity of 3.6 μm s^{-1} (Fig. 11), comparable to the velocity, around 4 μm s^{-1}, of 175-kD myosin fixed on a glass surface in vitro (Tominaga et al., 2003). From these results, we propose that the movement of 175-kD myosin associated with ER along the actin filament is one of the mechanisms responsible for the formation of cortical ER tubules and their networks in the S12 fraction and also in vivo. BY-2 myosin VIII-1 appeared to possess motile activity (Supplemental Fig. S12), although the sliding velocity of F-actin by this myosin in vitro was slower than that by myosin XI. From the immunodepletion experiment (Fig. 7), BY-2 myosin VIII-1 is demonstrated to be not responsible for ER tubule formation in the S12 fraction.

Model for Functions of Myosin XI and Actin in ER Remodeling in Vivo

The dynamic behavior of actin, the polymerization and the elongation of actin filaments from preexisting filaments, shortening by severing activity, buckling, and straightening behaviors of filaments were shown in the cortex of Arabidopsis epidermal cells (Staiger et al., 2009). When actin filaments are polymerized and elongate near the cortical ER elements, the 175-kD myosin associated with the ER membrane slides along

these actin filaments, hauling the ER membrane, resulting in the elongation of ER tubules. The dynamics of actin, especially the polymerization to actin filaments in the cortical region, may play a crucial role in regulating the sliding movement of myosin XI and consequently the organization of the ER network. We could not exclude another potential mechanism in in vivo ER tubule elongation, a pushing force by the polymerization of actin, as proposed by Sparkes et al. (2009a), although such a mechanism appears to be not exerted in the S12 fraction used in this study (Supplemental Fig. S5).

In this study, we showed that the 175-kD myosin, a BY-2 homolog of myosin XI-2 of Arabidopsis or *N. benthamiana*, generates the force for the elongation of ER tubules. This myosin was previously indicated to contribute to ER transport (Yokota et al., 2009). Recently, Arabidopsis myosin XI-K was revealed to be a primary contributor to ER transport and streaming in Arabidopsis, whereas the contributions of myosin XI-1 and XI-2 were more limited (Ueda et al., 2010). The C-terminal tail of Arabidopsis myosin XI-K overexpressed in tobacco cells caused the suppression of cortical ER network dynamics (Sparkes et al., 2009a). The BY-2 homolog of myosin XI-K, the 170-kD myosin, appeared to be localized to dot-like organelles but not to ER in BY-2 cells (Yokota et al., 2009). These observations imply that several members of myosin XI are involved in ER transport and streaming and raise the possibility that the main contributor to these events among these myosin XI members is species specific. Furthermore, it is attractive to assume that the primary myosin XI member responsible for ER transport is also involved in the dynamics of cortical ER networks in plant cells. The in vitro ER tubule formation assay using the S12 fraction prepared from a mutant strain in which certain myosin XI isoforms are depleted will help to determine the isoform(s) of myosin XI responsible for the formation of ER tubules in Arabidopsis.

MATERIALS AND METHODS

Preparation of Proteins and Antibodies

F-actin and microtubules were prepared from chicken breast muscle according to the method of Kohama (1981) and from BY-2 cells according to the method of Hamada et al. (2004), respectively. Microtubules were stabilized by 20 μM taxol. F-actin and microtubules were stained with RP and Oregon Green 488 taxol (Invitrogen), respectively, allowing them to be visualized by fluorescence microscopy.

The anti-175-kD myosin antibody was raised against the C-terminal 100 amino acids (Supplemental Fig. S1, blue double arrow; Tominaga et al., 2003) and used as the anti-BM175 tail antibody in this study. A polypeptide of 19 amino acids in the 175-kD myosin H chain (RTNDAPSFTPSKNYETPDS, corresponding to amino acids 937–955; Supplemental Fig. S1, red double arrow) coupled with keyhole limpet hemocyanin was purchased from Qiagen. It was mixed with Titer Max Gold (TiterMax USA) and injected into a male rabbit. A total of three boosts were given at 2-week intervals. The animal was bled 2 weeks after the final injection. The serum was used as an anti-BM175 peptide antibody.

The antibody was raised against a recombinant myosin VIII H chain, amino acids 1,008 to 1,166 of Arabidopsis (*Arabidopsis thaliana*) ATM1. cDNA encoding ATM1 (clone name C104705) was obtained from the Arabidopsis Biological Resource Center (http://abrc.osu.edu/index.html). The tail region of the ATM1 H chain was amplified by PCR using ATM1 tail-specific primers (forward, 5′-CGGGATCCAAGCAAATGAGGTCGTTGCAG-3′; reverse, 5′-TCCCCCGGGCTGCAGATACCTGGTGCTATTTCTCCT-3′). The amplified product was digested with *Bam*HI and *Pst*I and ligated to *Bam*HI/*Pst*I-restricted pQE30 vector (Qiagen). The expression vector was transformed into *Escherichia coli* BL21 (DE3) plysS (Invitrogen). The transformants were grown in 900 mL of Luria-Bertani medium at 37°C until they reached an optical density of 0.5 at 600 nm, following which expression was induced by 0.5 mM isopropyl-β-D-thiogalactopyranoside. The tail region (amino acids 1,008–1,166) of ATM1, fused His-6 tag at its N-terminal region, was purified through a nickel-Sepharose column according to the manufacturer's protocol (GE Healthcare). After washing, the protein was eluted using 20 mM phosphate buffer (pH 7.4) containing 100 mM imidazole. The antibody was prepared by the method described above and used as an anti-ATM1 antibody.

Culture of BY-2 Cells and Isolation of the ER Fraction

Tobacco (*Nicotiana tabacum*) BY-2 cells, in which an ER-specific retention signal, HDEL, tagged with GFP was stably expressed (Mitsuhashi et al., 2000), were cultured by the method of Nagata et al. (1981). The cells were collected by centrifugation at 1,500*g* for 2 min and suspended in a solution containing 1% cellulase Onozuka RS (Yakult), 0.2% pectolyase Y23 (Seishin Pharmaceutical), and 0.45 M mannitol (pH 5.5). After 1.5 to 2 h, protoplasts were collected by centrifugation and washed three times with 0.6 M mannitol. GFP-ER vesicle was isolated from protoplasts by Suc density gradient ultracentrifugation according to the method of Dong et al. (1988) with some modifications. The following procedures were carried out at 0°C to 4°C. Protoplasts were homogenized in 3 volumes of a homogenization buffer (8 mM EGTA, 1 mM $MgCl_2$, 0.5% casein, 0.35 M Suc, 0.5 mM dithiothreitol [DTT], 1 mM phenylmethylsulfonyl fluoride [PMSF], 50 μg mL^{-1} leupeptin, and 40 mM PIPES-KOH [pH 7.0]) using a hand-operated Downs homogenizer. Cell breakage was monitored by microscopy. Supplemental Figure S2 shows a schematic of the isolation steps of the S12 fraction and GFP-ER vesicles. The homogenate was centrifuged at 2,000*g* for 3 min. The supernatant was further centrifuged at 12,000*g* for 10 min. The supernatant (Supplemental Fig. S2, S12 fraction) containing the microsomal fraction and cytosol was centrifuged on a 0.6 M, 1.0 M, and 1.5 M discontinuous Suc density gradient made up in an EMP solution (5 mM EGTA, 1 mM $MgCl_2$, 0.5 mM DTT, 1 mM PMSF, 50 μg mL^{-1} leupeptin, and 30 mM PIPES-KOH [pH 7.0]) at 86,000*g* for 1.5 h The interface between 1.0 and 1.5 M Suc was recovered, and the GFP-ER vesicles were used in our study (Supplemental Fig. S2). The protein concentration of GFP-ER vesicles, which was determined by the method of Bradford (1976), was approximately 0.65 to 0.75 mg mL^{-1}. The GFP-ER vesicles were diluted 2- to 4-fold with EMP solution and used in the experiment described below. To further remove the peripheral membrane proteins, GFP-ER vesicles were diluted 2-fold with the EMP solution supplemented with 0.6 M KCl. After centrifugation at 126,000*g* for 20 min, the pellet was suspended in the EMP solution supplemented with 0.4 M Suc.

Observation of ER Tubule Elongation from GFP-ER Vesicles

GFP-ER vesicles were mixed with GTP at various concentrations at 25°C and then observed by laser scanning microscopy (LSM-510 or Axioplan 2 Imaging [Carl Zeiss] equipped with a CSU 10 confocal laser scanning unit [Yokogawa Electric]) or a conventional fluorescence microscope (BH-2; Olympus) equipped with epifluorescence optics. Instead of GTP, GDP, ATP, or GTPγS at a final concentration of 0.5 mM was added to GFP-ER vesicles. To examine the effect of biotin-maleimide on tubule elongation, this drug at a final concentration of 10 μM was mixed with GFP-ER vesicles prepared without 0.5 mM DTT and kept standing at 25°C. After 10 min, DTT at a final concentration of 0.5 mM was added to the mixture, and further GTP was added. For analyzing the role of shearing force in tubule elongation, GFP-ER vesicles were supplemented with 0.5 mM GTP on ice and introduced on ice into a flow chamber, which was made from a glass slide and a coverslip separated from each other by two strips of tape. The sample was kept standing at 25°C for 10 min, then visualized. The flow was generated by the adsorption of solution from the flow chamber with a filter paper. Images were recorded through a high-sensitivity CCD camera (ORCA-ER C4742-80 or EM-CCD camera C9100; Hamamatsu Photonics).

Measurement of GTPase Activity

The GRP-ER vesicles were diluted 3-fold with EMP solution. GTP at a final concentration of 0.4 mM was added to the diluted GFP-ER vesicles, and the mixture was kept standing at 25°C. After the desired times, perchloric acid at a final concentration of 0.6 M was added to the mixture to terminate the reaction. The amount of Pi liberated was determined by the method of Kodama et al. (1986). For analyzing the GTPase activity during tubule formation, the mixture of GFP-ER vesicles with 0.4 mM GTP was continuously stirred using a magnetic stirrer during the reaction.

Motile Activity of Myosin VIII from BY-2 Cells

Each procedure was performed at 0°C to 4°C. BY-2 protoplasts were homogenized with a motor-driven glass-Teflon homogenizer in solution A (20 mM EGTA, 2 mM $MgCl_2$, 2 mM DTT, 100 μg mL^{-1} leupeptin, 1 mM PMSF, and 30 mM PIPES-KOH [pH 7.0]) supplemented with 1% casein and 0.25 M Suc. After centrifugation at 10,000*g* for 10 min, the supernatant was further centrifuged at 100,000*g* for 30 min. F-actin at a final concentration of 0.1 mg mL^{-1} was added to the resultant supernatant. The mixture was kept on ice for 30 min. After centrifugation at 100,000*g* for 30 min, the pellet referred to as a coprecipitant with F-actin was suspended in solution A supplemented with 10 mM ATP and 5 mM potassium phosphate buffer (pH 7.0) and kept on ice for 20 min. After centrifugation at 100,000*g* for 30 min, the pellet was recovered and resuspended in solution A supplemented with 0.3 M KCl and kept on ice for 20 min. After centrifugation at 100,000*g* for 30 min, the pellet was resuspended in solution A supplemented with 0.2 M KCl, 10 mM ATP, and 5 mM potassium phosphate buffer (pH 7.0) and kept on ice for 20 min. After centrifugation at 100,000*g* for 30 min, the supernatant (KCl-ATP extract from F-actin coprecipitant) was recovered and applied to a hydroxylapatite column (Bio-Rad) preequilibrated with solution A containing 0.2 M KCl. The adsorbed materials were eluted over a linear concentration gradient of 100 to 350 mM potassium phosphate buffer (pH 7.0) in preequilibration solution. Fractions containing the 130-kD component detected by immunoblotting with the anti-ATM1 antibody were pooled and then dialyzed against solution B (30 mM KCl, 5 mM EGTA, 2 mM $MgCl_2$, 1 mM DTT, 50 μg mL^{-1} leupeptin, 1 mM PMSF, and 20 mM PIPES-KOH [pH 7.0]). The dialysate was applied to a DEAE-Sephacel column (Amersham Biosciences) preequilibrated with the dialysis solution. The adsorbed materials were eluted over a linear concentration gradient of 30 to 600 mM KCl in preequilibrated solution. Fractions containing the 130-kD component were pooled and used in the in vitro motility assay according to a method of Yokota and Shimmen (1994).

For immunodepletion of the 130-kD component from the DEAE-Sephacel fraction, a protein A bead (nProtein A Sepharose; GE Healthcare) conjugated with the anti-ATM1 antibody was prepared. The anti-ATM1 antibody, diluted 50-fold with BSA supplemented with 0.05% (v/v) Tween 20 and 2% (w/v) BSA, was mixed with one-tenth volume of protein A beads at 4°C for 1 h. After washing several times with solution B, the beads were mixed with the DEAE-Sephacel fraction at 4°C for 1 h. After centrifugation at 500*g* for 20 s, the supernatant and the pellet containing beads were recovered and subjected to SDS-PAGE according to the method of Laemmli (1970). The proteins in the gel were electrophoretically transferred to a polyvinylidene fluoride-nitrocellulose sheet (Immobilon-P; Millipore) according to the method of Towbin et al. (1979) for immunoblotting. The other portion of the supernatant was used for the in vitro motility activity. As a control, the anti-BM175 tail antibody was used and treated in a similar manner to that described above.

Observation of ER Tubule Elongation in the S12 Fraction

The S12 fraction was diluted 2-fold with 0.35 M Suc solution (0.35 M Suc, 5 mM EGTA, 1 mM $MgCl_2$, 0.5 mM DTT, 1 mM PMSF, 50 μg mL^{-1} leupeptin, and 30 mM PIPES-KOH [pH 7.0]) supplemented with GTP, ATP, and F-actin at final concentrations of 0.5 mM, 2 mM, and 2.5 μg mL^{-1}, respectively, on ice, and the mixture was introduced into the flow chamber on ice. The sample was kept standing at 25°C for 30 to 50 min and observed by fluorescence microscopy. Instead of F-actin, taxol-stabilized microtubules at a final concentration of 8 μg mL^{-1} were added to the diluted S12 fraction with taxol at a final concentration of 20 μM. To quantify the extent of ER tubule formation under various conditions, the total length of tubules in a 90-μm × 90-μm field was measured, and an average length of 10 fields was calculated. To deplete myosin from the S12 fraction, a one-fiftieth volume of the anti-BM175 tail, the anti-BM175 peptide, or the anti-ATM1 antibody was added to the S12 fraction and suspended at 4°C. After 1 h, a one-sixth volume of protein A beads was further added to the mixture and suspended at 4°C for 1 h. After centrifugation at 500*g* for 20 s, the supernatant was recovered. The pellet containing beads was washed several times with EMP solution. One portion of supernatant and beads was subjected to SDS-PAGE and then immunoblotting. As a control, the S12 fraction was mixed only with protein A beads but not the antibody. To examine the formation of ER tubules, another portion of the supernatant was diluted 2-fold with 0.35 M Suc solution as described above.

To reduce the amount of G-actin in the S12 fraction, Affi-Gel 10 beads (Bio-Rad) conjugated covalently with DNase I (Roche Diagnostics) were prepared according to the method of Yokota et al. (2005) and used as DNase I beads. Beads conjugated with BSA were used as a control. A one-tenth volume of the beads was added to the S12 fraction and suspended on ice for 40 min. After centrifugation at 500*g* for 20 s, the supernatant was recovered. One portion was diluted 2-fold with 0.35 M Suc solution as described above for analyzing tubule formation. Another portion was subjected to SDS-PAGE with various concentrations of chicken actin and then immunoblotted with an antibody against actin (clone C4; MP Biomedicals). S12 fractions either untreated or treated with the BSA beads were diluted 4-fold before their application on SDS-PAGE.

To examine the effect of myosin XI tail on tubule elongation, a 100-amino acid C-terminal recombinant 175-kD myosin H chain tail protein, whose C terminus was fused to dihydrofolate reductase (Tominaga et al., 2003) at a concentration of 20 μg mL^{-1}, was added to the S12 fraction and suspended at 4°C. After 1 h, one portion of the mixture was diluted 2-fold with 0.35 M Suc solution as described above for analyzing tubule formation. Another portion of the mixture was centrifuged at 180,000*g* for 20 min at 2°C. The supernatant and pellet were subjected to SDS-PAGE and immunoblotting. As a control recombinant protein, an unrelated 100-amino acid polypeptide with myosin (DPNYSLLNQTVNPDITMRQHFKQLGPINISNECINQEIQKTFTNPSFKN-PTSHQMSLTGNLCSSNDNSKKEMMDVCMLEADWIETCSEFSQGHSQK-SWSPINK), which is linked dihydrofolate reductase, was used and added to the S12 fraction at a concentration of 25 μg mL^{-1}.

MS

The S12 fraction, ATP extract, or KCl extract from F-actin coprecipitant was mixed with the anti-ATM1 antibody, the anti-BM175 tail, or the anti-BM175 peptide antibody and then further with protein A beads. After washing the beads several times, they were subjected to SDS-PAGE and immunoblotting with those antibodies. The cross-reacting bands with each antibody were excised from the gels and subjected to MS analysis at Japan Bio Services.

Immunoblotting

Antigens on the nitrocellulose membrane were detected as described previously (Yokota et al., 1995). The anti-BM175 tail, anti-BM175 peptide, anti-ATM1, anti-actin antibody, or alkaline phosphatase-conjugated anti-rabbit IgG (Sigma) was diluted 500-, 500-, 500-, 500-, or 3,000-fold, respectively, with phosphate-buffered saline supplemented with 2% (w/v) BSA and 0.05% (v/v) Tween 20. Band intensity was measured by densitometry (Densito-pattern analyzer EPA-3000; Cosmo Bio.).

Supplemental Data

The following materials are available in the online version of this article.

Supplemental Figure S1. Sequences of C-terminal tail regions of myosin heavy chains in class XI.

Supplemental Figure S2. Isolation protocol of the S12 fraction and GFP-ER vesicles from BY-2 cells.

Supplemental Figure S3. Elongation of tubules from GFP-ER vesicles.

Supplemental Figure S4. The presence of actin-binding protein, villin, in the S12 fraction, and the arrangement of added F-actin into bundles.

Supplemental Figure S5. Reduction of G-actin concentrations, including endogenously, in the S12 fraction by DNase I beads.

Supplemental Figure S6. Exogenous microtubules did not induce the formation of ER tubules in the S12 fraction.

Supplemental Figure S7. Presence of the 130-kD component in Arabidopsis seedling and the S12 fraction of BY-2 cells.

Supplemental Figure S8. MS analyses of immunoprecipitates with myosin antibodies in the S12 fraction.

Supplemental Figure S9. Dissociation of BY-2 myosin VIII-1 from F-actin by ATP.

Supplemental Figure S10. Preparation of BY-2 myosin VIII-1 from the eluate of ATP-containing high-ionic-strength solution by a hydroxylapatite and then DEAE-Sephacel column chromatography.

Supplemental Figure S11. DEAE-Sephacel fraction containing BY-2 myosin VIII-1 and immunoprecipitation with the anti-ATM1 antibody.

Supplemental Figure S12. Motile activity in vitro in the supernatant after immunoprecipitation.

Supplemental Figure S13. The immunodepletion of 175-kD myosin with the anti-BM175 peptide antibody from the S12 fraction.

Supplemental Figure S14. A recombinant C-terminal tail region of the 175-kD myosin H chain.

ACKNOWLEDGMENTS

We thank the National Live Stock Breeding Center Hyogo Station for the gift of chicken breast muscle.

Received February 22, 2011; accepted March 18, 2011; published March 22, 2011.

LITERATURE CITED

Audhya A, Desai A, Oegema K (2007) A role for Rab5 in structuring the endoplasmic reticulum. J Cell Biol **178:** 43–56

Avisar D, Prokhnevsky AI, Makarova KS, Koonin EV, Dolja VV (2008) Myosin XI-K is required for rapid trafficking of Golgi stacks, peroxisomes, and mitochondria in leaf cells of *Nicotiana benthamiana*. Plant Physiol **146:** 1098–1108

Boevink P, Oparka K, Santa Cruz S, Martin B, Betteridge A, Hawes C (1998) Stacks on tracks: the plant Golgi apparatus traffics on an actin/ER network. Plant J **15:** 441–447

Bradford MM (1976) A rapid and sensitive method for the quantitation of microgram quantities of protein utilizing the principle of protein-dye binding. Anal Biochem **72:** 248–254

Brandizzi F, Snapp EL, Roberts AG, Lippincott-Schwartz J, Hawes C (2002) Membrane protein transport between the endoplasmic reticulum and the Golgi in tobacco leaves is energy dependent but cytoskeleton independent: evidence from selective photobleaching. Plant Cell **14:** 1293–1309

Dong JG, Satoh S, Fujii T (1988) Variation in endoplasmic reticulum-associated glycoproteins of carrot cells cultured *in vitro*. Planta **173:** 419–423

Dreier L, Rapoport TA (2000) In vitro formation of the endoplasmic reticulum occurs independently of microtubules by a controlled fusion reaction. J Cell Biol **148:** 883–898

Estrada P, Kim J, Coleman J, Walker L, Dunn B, Takizawa P, Novick P, Ferro-Novick S (2003) Myo4p and She3p are required for cortical ER inheritance in *Saccharomyces cerevisiae*. J Cell Biol **163:** 1255–1266

Foissner I, Menzel D, Wasteneys GO (2009) Microtubule-dependent motility and orientation of the cortical endoplasmic reticulum in elongating characean internodal cells. Cell Motil Cytoskeleton **66:** 142–155

Galway ME, Heckman JW Jr, Schiefelbein JW (1997) Growth and ultrastructure of *Arabidopsis* root hairs: the *rhd3* mutation alters vacuole enlargement and tip growth. Planta **201:** 209–218

Golomb L, Abu-Abied M, Belausov E, Sadot E (2008) Different subcellular localization and functions of Arabidopsis myosin VIII. BMC Plant Biol **8:** 1–13

Hachikubo Y, Ito K, Schiefelbein J, Manstein DJ, Yamamoto K (2007) Enzymatic activity and motility of recombinant *Arabidopsis* myosin XI, MYA1. Plant Cell Physiol **48:** 886–891

Hamada T, Igarashi H, Itoh TJ, Shimmen T, Sonobe S (2004) Characterization of a 200 kDa microtubule-associated protein of tobacco BY-2 cells, a member of the XMAP215/MOR1 family. Plant Cell Physiol **45:** 1233–1242

Hashimoto K, Igarashi H, Mano S, Takenaka C, Shiina T, Yamaguchi M, Demura T, Nishimura M, Shimmen T, Yokota E (2008) An isoform of *Arabidopsis* myosin XI interacts with small GTPases in its C-terminal tail region. J Exp Bot **59:** 3523–3531

Higaki T, Kutsuna N, Sano T, Hasezawa S (2008) Quantitative analysis of changes in actin microfilament contribution to cell plate development in plant cytokinesis. BMC Plant Biol **8:** 1–15

Hu J, Shibata Y, Zhu P-P, Voss C, Rismanchi N, Prinz WA, Rapoport TA, Blackstone C (2009) A class of dynamin-like GTPases involved in the generation of the tubular ER network. Cell **138:** 549–561

Hwang H-H, Gelvin SB (2004) Plant proteins that interact with VirB2, the *Agrobacterium tumefaciens* pilin protein, mediate plant transformation. Plant Cell **16:** 3148–3167

Jing Y, Yi K, Ren H (2003) Actins from plant and animal sources tend not to form heteropolymers in vitro and function differently in plant cells. Protoplasma **222:** 183–191

Kachar B, Reese TS (1988) The mechanism of cytoplasmic streaming in characean algal cells: sliding of endoplasmic reticulum along actin filaments. J Cell Biol **106:** 1545–1552

Kodama T, Fukui K, Kometani K (1986) The initial phosphate burst in ATP hydrolysis by myosin and subfragment-1 as studied by a modified malachite green method for determination of inorganic phosphate. J Biochem **99:** 1465–1472

Kohama K (1981) Amino acid incorporation rates into myofibrillar proteins of dystrophic chicken skeletal muscle. J Biochem **90:** 497–501

Knebel W, Quader H, Schnepf E (1990) Mobile and immobile endoplasmic reticulum in onion bulb epidermis cells: short- and long-term observations with a confocal laser scanning microscope. Eur J Cell Biol **52:** 328–340

Laemmli UK (1970) Cleavage of structural proteins during the assembly of the head of bacteriophage T4. Nature **227:** 680–685

Lee C, Chen LB (1988) Dynamic behavior of endoplasmic reticulum in living cells. Cell **54:** 37–46

Lichtscheidl IK, Lancelle SA, Hepler PK (1990) Actin-endoplasmic reticulum complexes in *Drosera*: their structural relationship with the plasmalemma, nucleus, and organelles in cells prepared by high pressure freezing. Protoplasma **155:** 116–126

Lichtscheidl IK, Url WG (1990) Organization and dynamics of cortical endoplasmic reticulum in inner epidermal cells of onion bulb scales. Protoplasma **157:** 203–215

Liebe S, Menzel D (1995) Actomyosin-based motility of endoplasmic reticulum and chloroplasts in *Vallisneria* mesophyll cells. Biol Cell **85:** 207–222

Menzel D (1994) Dynamics and pharmacological perturbations of the endoplasmic reticulum in the unicellular green alga Acetabularia. Eur J Cell Biol **64:** 113–119

Mitsuhashi N, Shimada T, Mano S, Nishimura M, Hara-Nishimura I (2000) Characterization of organelles in the vacuolar-sorting pathway by visualization with GFP in tobacco BY-2 cells. Plant Cell Physiol **41:** 993–1001

Nagata T, Okada K, Takebe I, Matsui C (1981) Delivery of tobacco mosaic virus RNA into plant protoplasts mediated by reverse-phase evaporation vesicle (liposomes). Mol Gen Genet **184:** 161–165

Nunokawa SY, Anan H, Shimada K, Hachikubo Y, Kashiyama T, Ito K, Yamamoto K (2007) Binding of *Chara* myosin globular tail domain to phospholipid vesicles. Plant Cell Physiol **48:** 1558–1566

Nziengui H, Bouhidel K, Pillon D, Der C, Marty F, Schoefs B (2007) Reticulon-like proteins in *Arabidopsis thaliana*: structural organization and ER localization. FEBS Lett **581:** 3356–3362

Nziengui H, Schoefs B (2009) Functions of reticulons in plants: what we can learn from animals and yeasts. Cell Mol Life Sci **66:** 584–595

Quader H (1990) Formation and disintegration of cisternae of the endoplasmic reticulum visualized in live cells by conventional fluorescence and confocal laser scanning microscopy: evidence for the involvement of calcium and the cytoskeleton. Protoplasma **155:** 166–175

Quader H, Hofmann A, Schnepf E (1987) Shape and movement of the endoplasmic reticulum in onion bulb epidermis cells: possible involvement of actin. Eur J Cell Biol **44:** 17–26

Quader H, Hofmann A, Schnepf E (1989) Reorganization of the endoplasmic reticulum in epidermal cells of onion bulb scales after cold stress: involvement of cytoskeletal elements. Planta **177:** 273–280

Reddy ASN, Day IS (2001) Analysis of the myosin encoded in the recently completed *Arabidopsis thaliana* genome sequence. Genome Biol **2:** 0024.1–0024.17

Reichelt S, Knight AE, Hodge TP, Baluska F, Samaj J, Volkmann D, Kendrick-Jones J (1999) Characterization of the unconventional myosin VIII in plant cells and its localization at the post-cytokinetic cell wall. Plant J **19:** 555–567

Ren H, Gibbon BC, Ashworth SL, Sherman DM, Yuan M, Staiger CJ (1997) Actin purified from maize pollen functions in living plant cells. Plant Cell **9:** 1445–1457

Runions J, Brach T, Kühner S, Hawes C (2006) Photoactivation of GFP reveals protein dynamics within the endoplasmic reticulum membrane. J Exp Bot **57:** 43–50

Sparkes I, Runions J, Hawes C, Griffing L (2009a) Movement and remodeling of the endoplasmic reticulum in nondividing cells of tobacco leaves. Plant Cell **21:** 3937–3949

Sparkes I, Tolley N, Aller I, Svozil J, Osterrieder A, Botchway S, Mueller C, Frigerio L, Hawes C (2010) Five *Arabidopsis* reticulon isoforms share endoplasmic reticulum location, topology, and membrane-shaping properties. Plant Cell **22:** 1333–1343

Sparkes IA, Frigerio L, Tolley N, Hawes C (2009b) The plant endoplasmic reticulum: a cell-wide web. Biochem J **423:** 145–155

Sparkes IA, Ketelaar T, de Ruijter NCA, Hawes C (2009c) Grab a Golgi: laser trapping of Golgi bodies reveals *in vivo* interactions with the endoplasmic reticulum. Traffic **10:** 567–571

Staehelin LA (1997) The plant ER: a dynamic organelle composed of a large number of discrete functional domains. Plant J **11:** 1151–1165

Staiger CJ, Sheahan MB, Khurana P, Wang X, McCurdy DW, Blanchoin L (2009) Actin filament dynamics are dominated by rapid growth and severing activity in the *Arabidopsis* cortical array. J Cell Biol **184:** 269–280

Terasaki M, Reese TS (1994) Interactions among endoplasmic reticulum, microtubules, and retrograde movements of the cell surface. Cell Motil Cytoskeleton **29:** 291–300

Tolley N, Sparkes IA, Hunter PR, Craddock CP, Nuttall J, Roberts LM, Hawes C, Pedrazzini E, Frigerio L (2008) Overexpression of a plant reticulon remodels the lumen of the cortical endoplasmic reticulum but does not perturb protein transport. Traffic **9:** 94–102

Tominaga M, Kojima H, Yokota E, Orii H, Nakamori R, Katayama E, Anson M, Shimmen T, Oiwa K (2003) Higher plant myosin XI moves processively on actin with 35 nm steps at high velocity. EMBO J **22:** 1263–1272

Towbin H, Staehelin T, Gordon J (1979) Electrophoretic transfer of proteins from polyacrylamide gels to nitrocellulose sheets: procedure and some applications. Proc Natl Acad Sci USA **76:** 4350–4354

Turner MD, Plutner H, Balch WE (1997) A Rab GTPase is required for homotypic assembly of the endoplasmic reticulum. J Biol Chem **272:** 13479–13483

Ueda H, Yokota E, Kutsuna N, Shimada T, Tamura K, Shimmen T, Hasezawa S, Dolja VV, Hara-Nishimura I (2010) Myosin-dependent endoplasmic reticulum motility and F-actin organization in plant cells. Proc Natl Acad Sci USA **107:** 6894–6899

Vedrenne C, Hauri H-P (2006) Morphogenesis of the endoplasmic reticulum: beyond active membrane expansion. Traffic **7:** 639–646

Voeltz GK, Prinz WA, Shibata Y, Rist JM, Rapoport TA (2006) A class of membrane proteins shaping the tubular endoplasmic reticulum. Cell **124:** 573–586

Wagner W, Brenowitz SD, Hammer JA III (2011) Myosin-Va transports the endoplasmic reticulum into the dendritic spines of Purkinje neurons. Nat Cell Biol **13:** 40–48

Wang H, Lockwood SK, Hoeltzel MF, Schiefelbein JW (1997) The *ROOT HAIR DEFECTIVE3* gene encodes an evolutionarily conserved protein with GTP-binding motifs and is required for regulated cell enlargement in *Arabidopsis*. Genes Dev **11:** 799–811

Waterman-Storer CM, Salmon ED (1998) Endoplasmic reticulum membrane tubules are distributed by microtubules in living cells using three distinct mechanisms. Curr Biol **8:** 798–806

Wedlich-Söldner R, Schulz I, Straube A, Steinberg G (2002) Dynein supports motility of endoplasmic reticulum in the fungus *Ustilago maydis*. Mol Biol Cell **13:** 965–977

Wöllert T, Weiss DG, Gerdes H-H, Kuznetsov SA (2002) Activation of myosin V-based motility and F-actin-dependent network formation of endoplasmic reticulum during mitosis. J Cell Biol **159:** 571–577

Yamamoto K (2007) Plant myosins VIII, XI, and XIII. *In* LC Coluccio, ed, Myosins: A Superfamily of Molecular Motors. Springer, Berlin, pp 375–390

Yamamoto K, Shimada K, Ito K, Hamada S, Ishijima A, Tsuchiya T, Tazawa M (2006) *Chara* myosin and the energy of cytoplasmic streaming. Plant Cell Physiol **47:** 1427–1431

Yokota E, McDonald AR, Liu B, Shimmen T, Palevitz BA (1995) Localization of a 170 kDa myosin heavy chain in plant cells. Protoplasma **185:** 178–187

Yokota E, Shimmen T (1994) Isolation and characterization of plant myosin from pollen tubes of lily. Protoplasma **177:** 153–162

Yokota E, Shimmen T (2011) Plant myosins. *In* B Liu, ed, The Plant Cytoskeleton. Springer, New York, pp 33–56

Yokota E, Tominaga M, Mabuchi I, Tsuji Y, Staiger CJ, Oiwa K, Shimmen T (2005) Plant villin, lily P-135-ABP, possesses G-actin binding activity and accelerates the polymerization and depolymerization of actin in a Ca^{2+}-sensitive manner. Plant Cell Physiol **46:** 1690–1703

Yokota E, Ueda S, Tamura K, Orii H, Uchi S, Sonobe S, Hara-Nishimura I, Shimmen T (2009) An isoform of myosin XI is responsible for the translocation of endoplasmic reticulum in tobacco cultured BY-2 cells. J Exp Bot **60:** 197–212

Yokota E, Vidali L, Tominaga M, Tahara H, Orii H, Morizane Y, Hepler PK, Shimmen T (2003) Plant 115-kDa actin-filament bundling protein, P-115-ABP, is a homologue of plant villin and is widely distributed in cells. Plant Cell Physiol **44:** 1088–1099

Yokota E, Yukawa C, Muto S, Sonobe S, Shimmen T (1999) Biochemical and immunocytochemical characterization of two types of myosins in cultured tobacco Bright Yellow-2 cells. Plant Physiol **121:** 525–534

Zheng H, Kunst L, Hawes C, Moore I (2004) A GFP-based assay reveals a role for RHD3 in transport between the endoplasmic reticulum and Golgi apparatus. Plant J **37:** 398–414